In Situ Infrared Microspectroscopy of ~850 Million-Year-Old Prokaryotic Fossils

MOTOKO IGISU,* SATORU NAKASHIMA, YUICHIRO UENO, STANLEY M. AWRAMIK, and SHIGENORI MARUYAMA

Department of Earth and Planetary Sciences, Tokyo Institute of Technology, O-okayama 2-12-1, Meguro, Tokyo 152-8551, Japan (M.I., S.M.); Department of Earth and Space Science, Osaka University, 1-1 Machikaneyama-cho, Toyonaka-shi, Osaka 560-0043, Japan (M.I., S.N.); Research Center for the Evolving Earth and Planets, Department of Environmental Science and Technology, Tokyo Institute of Technology, Post No. S2-17 Midori-ku, Yokohama-shi, Kanagawa 226-8503, Japan (Y.U.); and Department of Earth Science, University of California, Santa Barbara, California 93106 (S.A.)

***In situ* infrared (IR) and Raman microspectroscopy have been conducted on Neoproterozoic, organic-walled microfossils (prokaryotic fossils) in doubly polished, petrographic thin sections in order to detect their spectral signatures. The microfossils are very well preserved and occur in black chert from the ~850 million-year-old Bitter Springs Formation, Northern Territory, Australia. Raman microspectroscopy on two species of microfossils, one a filament and the other a coccoid, shows disordered peaks (D peak, 1340 cm^{-1}) and graphite peaks (G peak, 1600 cm^{-1}), indicating that they consist of disordered carbonaceous materials. IR micro-mapping results of the filament reveal that the distributions of peak heights at 2920 cm^{-1} (aliphatic CH_2), 1585 cm^{-1} (aromatic C–C), and 1370 cm^{-1} (aliphatic CH_3) match the shape of the filamentous microfossil. These results suggest that IR microspectroscopy can be used for *in situ* characterization of organic polar signatures that morphologically indicate microfossils embedded in chert by using doubly-polished rock (petrographic) thin section samples. Further, these methods can be applied to controversial microfossil-like structures to test their biogenic nature.**

Index Headings: **Fourier transform infrared spectroscopy; FT-IR spectroscopy; Raman; Microspectroscopy; Mapping; Microfossils; Bitter Springs Formation; Rock thin section.**

INTRODUCTION

The record of life in the Archean and Proterozoic (4030 to 542 Ma: million years ago) is dominated by microbial fossils and biosedimentary products of microbial activity (stromatolites). For microfossils, a variety of criteria have been used to recognize them and to establish their biogenic origin, the principle ones being: (1) the shapes resemble modern microorganisms (a "biology-like" morphology), (2) the shapes are not defined by crystal boundaries, (3) they are composed of carbonaceous material of biological origin, and (4) they were deposited with the original sediment (syngenetic with original sedimentation, i.e., not post-depositional contaminants).[1–3] Microfossils are known from rocks that range in degree of metamorphism from sub-greenschist (burial metamorphism) to amphibolite grade. Establishing the biogenicity and syngenicity of Archean microfossils has proven particularly challenging and controversial due to their great age and thermal histories.[1–9]

The morphology of ancient microfossils has attracted the greatest amount of attention. Modern analytical techniques are now being applied to assist in improving the confidence that a morphologically identified microfossil is, indeed, a *bona fide* microfossil. *In situ* laser Raman spectroscopy is one of the techniques being applied to microfossil-like, black to amber-brown objects in petrographic thin sections in order to determine whether they are composed of carbonaceous (biological) materials.[6–11] *In situ* analysis, therefore, is important to further characterize the evidence to support a biogenic origin of microfossils. Extraction of microfossils from the rock matrix by the commonly used palynological technique of acid maceration can destroy delicate microbial remains.[12] However, the Raman spectral signature of carbonaceous material generally shows only disordered carbonaceous structure, which might not necessarily have originated from the biomolecules.[13] Organic polar signatures from biomolecules cannot be obtained easily. Ancient microfossils might retain some additional molecular records derived from their original biological molecules, even when metamorphosed.

Infrared (IR) spectroscopy is frequently used to characterize polar functional groups in carbonaceous material.[14–17] Since biochemical constituents (lipids, proteins, sugars, nucleic acids, etc.) contain polar components such as C–H, C=O, N–H, C–O, C–N, and P–O,[13,18] it is desirable to detect any preserved polar functional group in the carbonaceous material of individual microfossils. So far, IR microspectroscopy has been used to analyze acritarchs (organic-walled microfossils of uncertain taxonomic affinity extracted from rock samples by palynological techniques[12]) and has revealed that different acritarch species can have different spectroscopic characteristics. IR microspectroscopy has also been applied to microscopic globules in a carbonaceous chondrite that fell in Tagish Lake, Canada, in 2000, indicating the presence of C–H, C=O, and C–O bonds.[22] However, IR spectroscopy has rarely been applied to small prokaryotic microfossils in ancient rocks, because spatial resolution of IR spectroscopy is worse than that of laser

Received 11 May 2006; accepted 10 July 2006.
* Author to whom correspondence should be sent. E-mail: migisu@ess.sci.osaka-u.ac.jp.

0003-7028/06/6010-1111$2.00/0

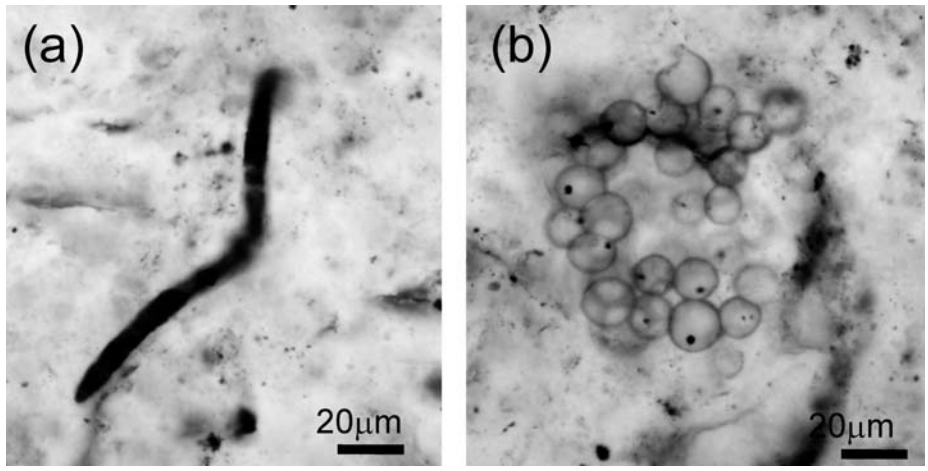

FIG. 1. Optical photomicrographs of (**a**) a filamentous microfossil and (**b**) coccoidal microfossils in a petrographic thin section of the black chert. Scale bar represents 20 μm.

Raman spectroscopy. Recent developments in IR microimaging have improved the spatial resolution of IR spectroscopy for characterization of biological and industrial materials,[23–26] for example, IR imaging has detected the distribution of organic signatures, such as amide I (1600 cm^{-1} absorption) in a single red blood cell.[24]

We report on a new approach for the characterization of molecular traces in prokaryotic microfossils preserved in chert by using *in situ* IR microspectroscopy together with Raman microspectroscopy on a doubly-polished petrographic thin section. This is the first report of *in situ* IR microspectroscopy conducted on prokaryotic fossils embedded in petrographic thin sections. Rather than first applying these methods to highly controversial Early Archean evidence of life (i.e., microstructures interpreted to be microbial fossils), the rationale was to apply this new method to unequivocal microfossils. The microbiota of the Neoproterozoic Bitter Springs Formation, one of the premier microfossil occurrences, provides an outstanding opportunity to test these new methods on fossils subjected to only burial metamorphism.[27] Applying these analytical methods to such well-preserved examples increases the confidence in use of their meaningful application to older, more challenging examples.

EXPERIMENTAL

Materials. The black chert sample from which the doubly-polished petrographic thin section was prepared was collected from the Loves Creek Member, Bitter Springs Formation, about 2 km NNW of Ross River Resort, 85 km east of Alice Springs, Northern Territory, Australia. The age of the Loves Creek Member is considered to be between 834 and 830 Ma.[28] Based on petrographic investigation of the thin section, the chert is composed mainly of microcrystalline quartz (SiO_2) with grain size primarily less than 10 μm. In descending order of abundance, the following was observed: quartz, brown to dark amber carbonaceous matter, microbial fossils (same color as carbonaceous matter), pyrite, iron-oxides, and carbonates. A poorly developed, irregularly laminated fabric is observed and defined by carbonaceous materials and occasionally by microbial fossils.

Bitter Springs Formation microfossils were first reported by Barghoorn and Schopf[29] and subsequently additional papers were published.[30,31] Two different microfossils were analyzed in this study, coccoids and a filament (Fig. 1). Both are three-dimensionally preserved in chert and are amber to dark brown in color. The filament (Fig. 1a) consists of a trichome with cells ~3 μm long and ~6 μm wide, with a well-developed tapered tip. The microfossil is assigned to *Cephalophytarion laticellulosum* based on cell size, terminal cell shape, and overall appearance.[31] The coccoids (Fig. 1b) are identified as *Glenobotrydion aenigmatis* based on cell size, eccentrically located dense "spot," occurrence in aggregates without envelope, and overall cell shape.[30] Both are interpreted as prokaryotic microfossils (cyanobacteria).[3,31]

Raman Microspectroscopy. Raman microspectroscopy was conducted on doubly-polished petrographic thin sections for the characterization of non-polar groups (e.g., C=C, S–S). A doubly-polished thin section was prepared as follows: A several-millimeters-thick rock chip, approximately 5 by 10 mm, was fashioned on a water-cooled diamond-blade rock saw. One surface was polished with #600, #1000, and #3000 alumina powder (28 μm, 16 μm, and 5 μm mean particle diameter, respectively) and alumina paste (<1 μm grain size) on a lapidary lap. This surface was attached to a glass slide using a carbon-based dissoluble adhesive (ARON ALPHA). The mounted chip was cut by a water-cooled, rock trim saw. The mounted chip was ground down and polished to about 40 μm in thickness with alumina powder on a lapidary lap. The other side of the rock section was then polished in the same way.

The polished thin section was exposed to an Ar laser (514.5 nm) for 5 seconds twice at a laser power of 20 mW to obtain Raman spectra in a range from 1800 to 200 cm^{-1} at 1 cm^{-1} resolution by using a laser Raman microspectrometer (Jasco NRS-2000). One measurement obtained a Raman spectrum with a range of about 800 cm^{-1} and spectra in the 1800–200 cm^{-1} range were obtained by combining two spectra. A 100× objective lens (NA = 0.84) was used so the spatial resolution of the Raman analysis was about 1–2 μm Φ. This also permitted accurate targeting of the microfossils, which occurred below the surface of the thin section, within the microcrystalline quartz (chert) matrix.

Infrared Microspectroscopy. Infrared microspectroscopy was used to characterize polar groups (e.g., C–H, C–N, C=O, O–H). After Raman microspectroscopic measurements, the doubly-polished rock chip (thin section) was removed from the

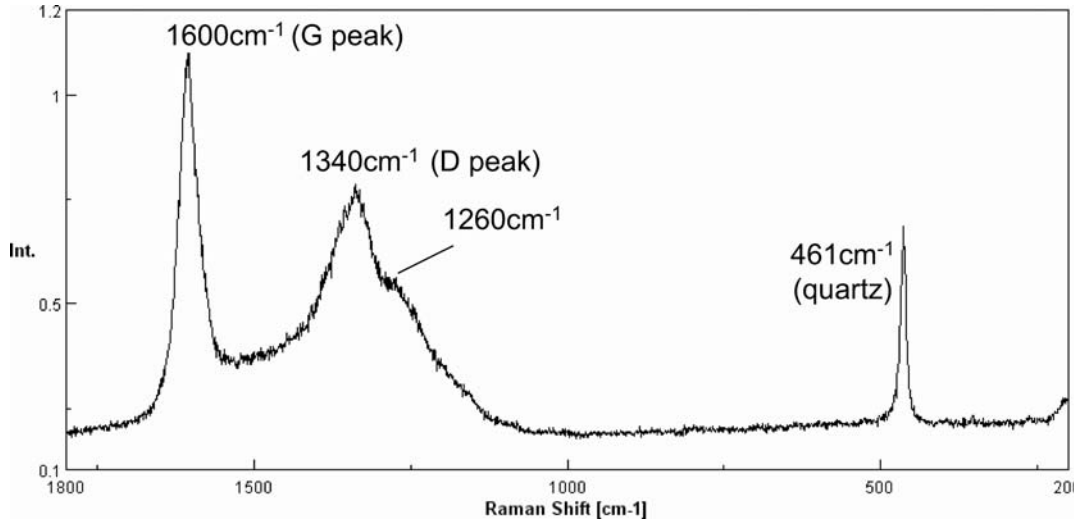

FIG. 2. A representative microscopic Raman spectrum of the microfossils in the chert. The bands around 1340 cm^{-1} (D peak) and 1600 cm^{-1} (G peak) are characteristic of disordered carbonaceous materials. The peak around 461 cm^{-1} is due to the quartz matrix of the chert.

glass slide by immersing it in acetone in order to dissolve the adhesive. Glass (slide) and the carbon-based adhesive (ARON ALPHA) would interfere with IR spectra of microfossils. The doubly-polished rock chip was placed over an opening in the sample holder. A rectangular aperture of 20 μm × 20 μm (an area of 400 μm^2) was used to select areas for the measurements. All IR transmission spectra were obtained by collecting 100 scans in a spectral range from 4000 to 700 cm^{-1} at 4 cm^{-1} resolution by using an IR microscope attached to an FT-IR spectrometer (Jasco FTIR620+IRT30). The IR microspectrometer used here does not have a sample chamber for purging with inactive gas. The IR microspectrometer stage was open to the atmosphere. The background spectrum was measured first without the sample (only air), and then the sample was measured to obtain the sample spectrum in absorbance. Analytical error was determined by duplicate measurements in the same position as the background spectrum. The analytical error in the range of 3500–2500 cm^{-1} was 0.01 absorbance unit (AU) and error in the range of 2300–1300 cm^{-1} was also 0.01 AU.

Infrared transmission spectra on the microfossils against air background were measured by collecting 1000 scans in a spectral range of 4000 to 1300 cm^{-1} at 4 cm^{-1} resolution in order to obtain more detailed spectral features. A few different rectangular apertures were used (15 μm × 50 μm and 25 μm × 25 μm) according to the microfossil sizes and IR signal intensities. IR transmission spectra of the quartz matrix without any amber to dark-brown microfossils or evident carbonaceous material were obtained for comparison with spectra of the microfossils. Spectral subtractions of the microfossils from the quartz matrix were then conducted to obtain the IR difference spectra with high signal-to-noise (S/N) ratio. Analytical error in the range of 3500–2500 cm^{-1} was 0.002 AU and error in the range of 2300–1300 cm^{-1} was 0.003 AU.

Infrared microspectroscopy was also conducted on the residues after acid treatments on the doubly-polished rock chip of the thin section in order to confirm the results of the above *in situ* IR spectra. The doubly-polished rock thin section was acid-treated by the following procedures. A drop of 27.5 N HF was put on the sample on a Pt plate (0.1 mm thick) with a pipette at room temperature. The residue was washed with distilled water and dried at room temperature for 3 days in

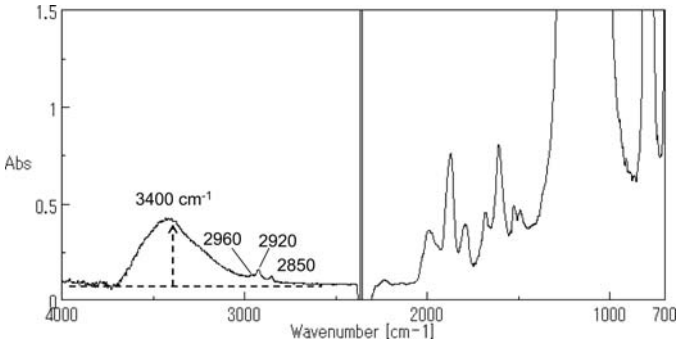

FIG. 3. A representative microscopic IR transmission spectrum against air background of the microfossils in the chert. Seven peaks (1995, 1870, 1793, 1684, 1610, 1525, and 1492 cm^{-1}) are overtones and combinations of Si–O bonds of quartz. The saturated bands (1400–700 cm^{-1}) are due to Si–O fundamental vibrations. The 3400 cm^{-1} broad band can be attributed to liquid-like molecular water (H_2O). The bands around 2920 and 2850 cm^{-1} are due to C–H stretching vibrations of mainly aliphatic CH_2 groups. The shoulder around 2960 cm^{-1} is due to C–H stretching of aliphatic CH_3 groups.

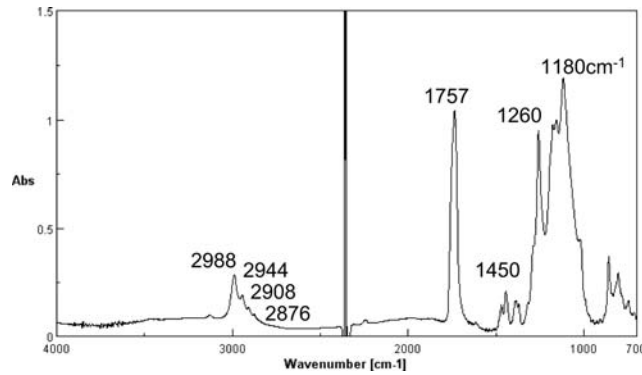

FIG. 4. IR transmission-reflection spectrum of the carbon-based dissolvable adhesive used in this study (ARON ALPHA) on an aluminum foil. The bands at 2988, 2944, 2908, and 2876 cm^{-1} are due to C–H stretching vibrations. The 1757 cm^{-1} band is due to ester C=O. The 1450 and 1375 cm^{-1} bands are due to C–H bending of $CH_2 + CH_3$ and CH_3 groups, respectively. The bands at 1260 and 1180 cm^{-1} are due to C–N and C–O, respectively.

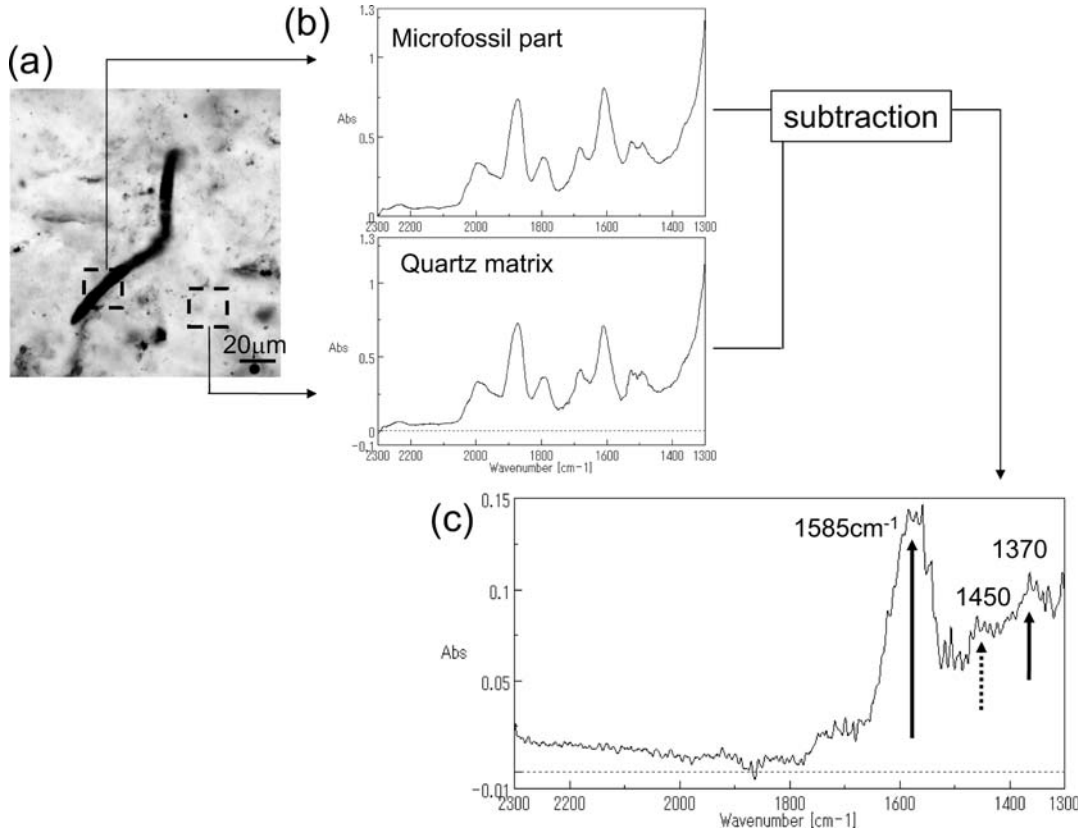

FIG. 5. Procedure for obtaining the IR difference spectrum of the microfossils subtracted from that of the quartz matrix. (**a**) Photomicrograph of the filamentous microfossil. Two boxes show measured areas (20×20 μm^2 square area) for the microfossil (left) and for the quartz matrix (right). (**b**) IR transmission spectra against air background of the microfossil and the quartz matrix. (**c**) The IR difference spectrum of the microfossil minus the quartz matrix. The bands around 1585 and 1370 cm^{-1} with a weak shoulder at 1450 cm^{-1} can be observed.

a draft chamber. The residue was then treated with 2 N HCl on the Pt plate, washed with distilled water, and dried at room temperature for 3 days in a draft chamber. IR transmission-reflection spectra of the residue on the Pt plate were obtained by collecting 1000 scans in the spectral range from 4000 to 700 cm^{-1} at 4 cm^{-1} resolution. The rectangular aperture for this measurement was 100 μm × 100 μm. The background transmission-reflection spectrum was measured on the Pt plate without the samples. Analytical error in the range of 3500–2500 cm^{-1} was 0.004 AU and error in the range of 2300–1300 cm^{-1} was 0.002 AU.

Infrared Mapping Analysis. Infrared mapping analysis was conducted on the doubly polished petrographic thin section using an automated X-Y mechanical stage attached to the IR spectrometer. The measured spectral range was from 4000 to 700 cm^{-1}. All IR transmission spectra were obtained

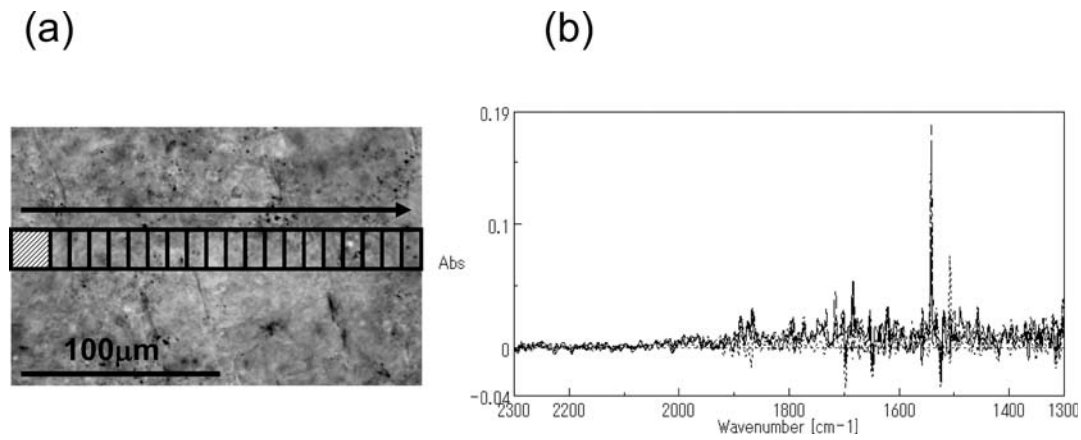

FIG. 6. IR line analysis for the quartz matrix. (**a**) Photomicrograph of the quartz matrix in the chert. The series of rectangles represent the areas measured (210×20 μm^2). The shaded square to the left is the reference quartz area (20×20 μm^2). The 20×20 μm^2 apertured area (open square) was shifted every 10 μm from left to right. (**b**) Typical IR difference spectra of the quartz matrix obtained from an area of quartz matrix (open square) minus the reference quartz area (shaded square). These do not show absorption bands in the range from 2300–1300 cm^{-1}, except for sharp noises.

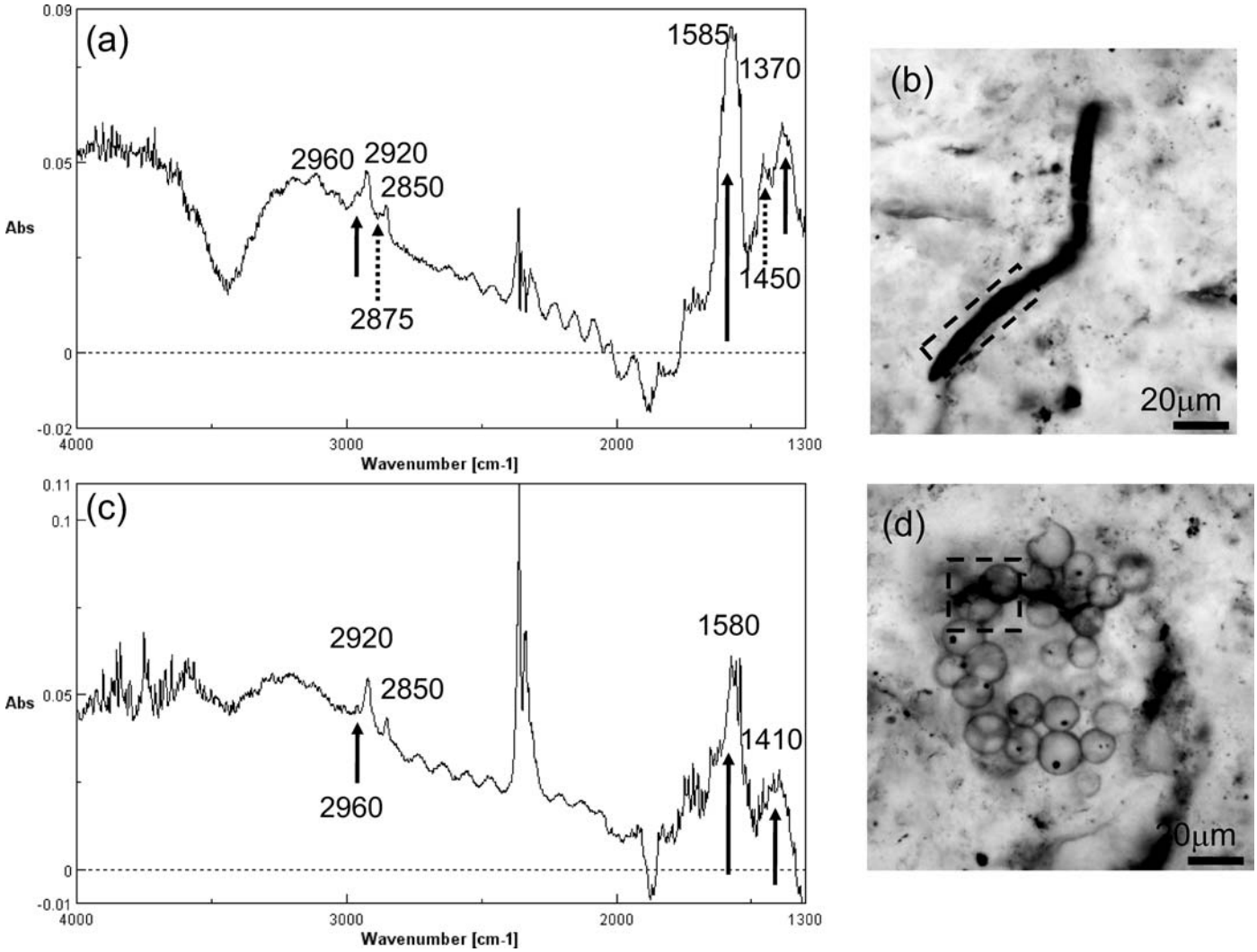

FIG. 7. The high S/N IR spectra (1000 scans) of the microfossils. (**a**) The high S/N IR spectrum of the filamentous microfossil minus the quartz matrix, showing the bands around 2960 cm^{-1} (CH_3), 2920 and 2850 cm^{-1} (CH2), 1585 cm^{-1} (aromatic C–C), 1450 cm^{-1} ($CH_2 + CH_3$), and 1370 cm^{-1} (CH_3). (**b**) Photomicrograph of the filamentous microfossil. The dashed rectangle shows the measured area (15×50 μm^2). (**c**) The high S/N IR spectra of the coccoidal microfossils minus the quartz matrix, showing the bands around 2960 cm^{-1} (CH_3), 2920 and 2850 cm^{-1} (CH_2), 1580 cm^{-1} (aromatic C–C), and 1410 cm^{-1} ($CH_2 + CH_3$). (**d**) Photomicrograph of the coccoidal microfossils. The dashed square shows the measured area (25×25 μm^2).

by collecting 100 scans against the air background. The 20 μm × 20 μm aperture was shifted every 10 μm for a 170 μm × 180 μm area. A total of 272 IR transmission spectra were obtained.

Infrared Line Analysis. Infrared line analysis was conducted on the doubly-polished thin section using the same system as the IR mapping analysis. All IR transmission spectra were obtained by collecting 100 scans in the 4000 to 700 cm^{-1} spectral range against the air background. The 20 μm × 20 μm aperture was linearly shifted every 10 μm in one direction for a 210 μm × 20 μm area. A total of 20 IR transmission spectra were obtained.

RESULTS

Raman Microspectroscopy. Raman spectroscopic analysis was conducted on microfossils three-dimensionally preserved in the quartz matrix. Most of the Raman spectra of the microfossils in this study showed three peaks (Fig. 2). The peak around 1600 cm^{-1} is called the graphite peak (G peak) and that around 1340 cm^{-1} with a shoulder at about 1260 cm^{-1}

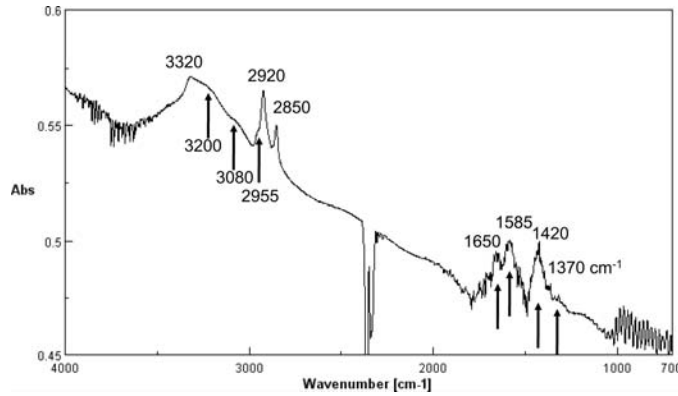

FIG. 8. A representative IR transmission-reflection spectrum of the residue on a Pt plate after HF/HCl dissolution of the doubly-polished petrographic thin section. The bands can be attributed as follows: 3320 cm^{-1} (N–H stretching), 3200 (alcoholic OH), 2960 cm^{-1} (aliphatic CH_3), 2920 and 2850 cm^{-1} (aliphatic CH_2), 1650 cm^{-1} (H–O–H bending), 1585 cm^{-1} (aromatic C–C), and 1420 cm^{-1} (aliphatic $CH_2 + CH_3$).

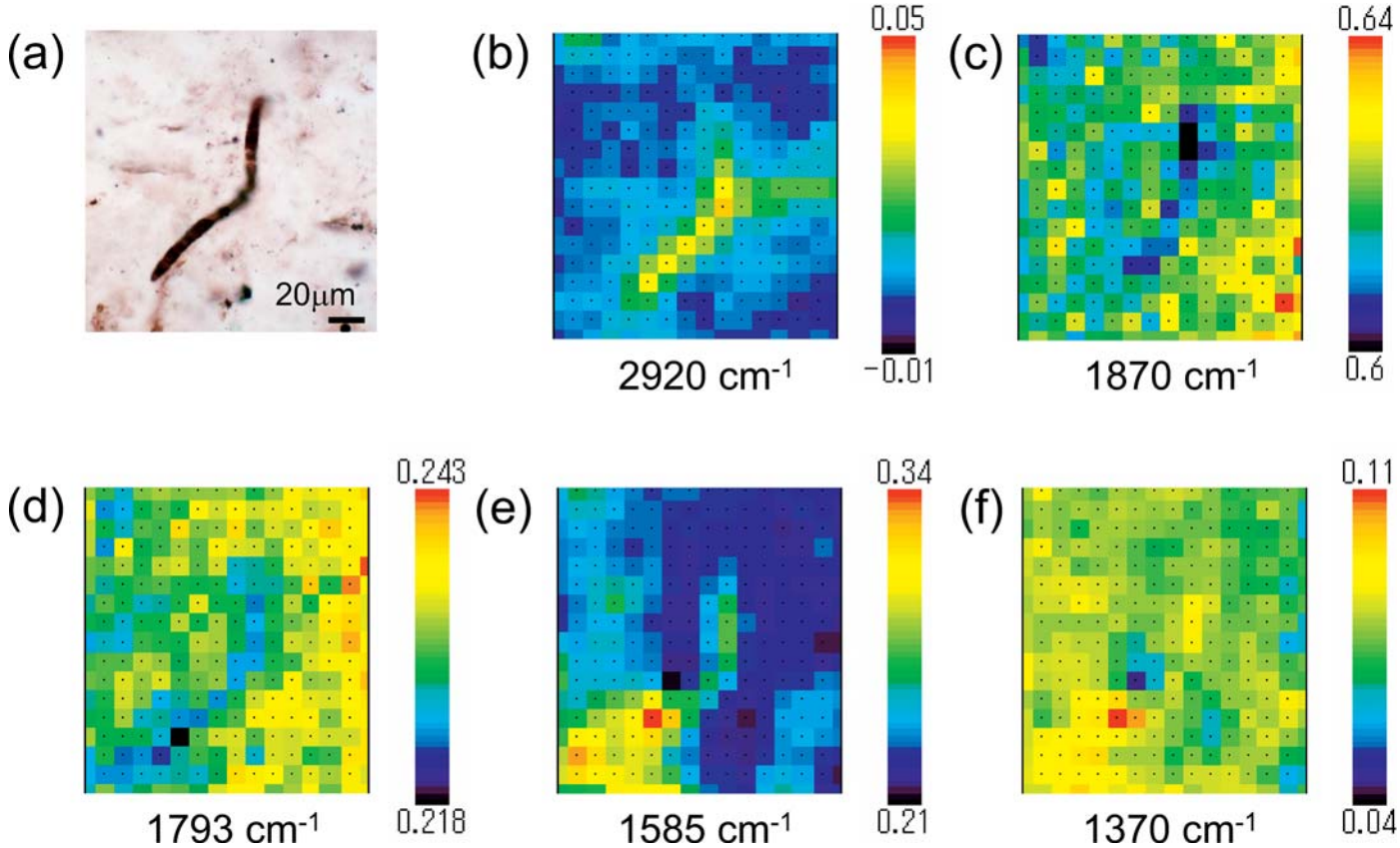

FIG. 9. IR mapping results by the raw IR transmission spectra (Fig. 3) of the filamentous microfossil embedded in the doubly-polished petrographic thin section. (**a**) Optical photomicrograph of the measured area (170×180 μm^2). Scale bar represents 20 μm. The spatial distribution maps for the peak heights at (**b**) 2920 cm^{-1} (C–H), (**c**) 1870 cm^{-1} (Si–O), (**d**) 1793 cm^{-1} (Si–O), (**e**) 1585 cm^{-1} (C–C), and (**f**) 1370 cm^{-1} (C–H). The color scale represents the higher peak height (red) and the lower one (blue) in absorbance units (AU). Analytical errors in absorbance are 0.01 AU.

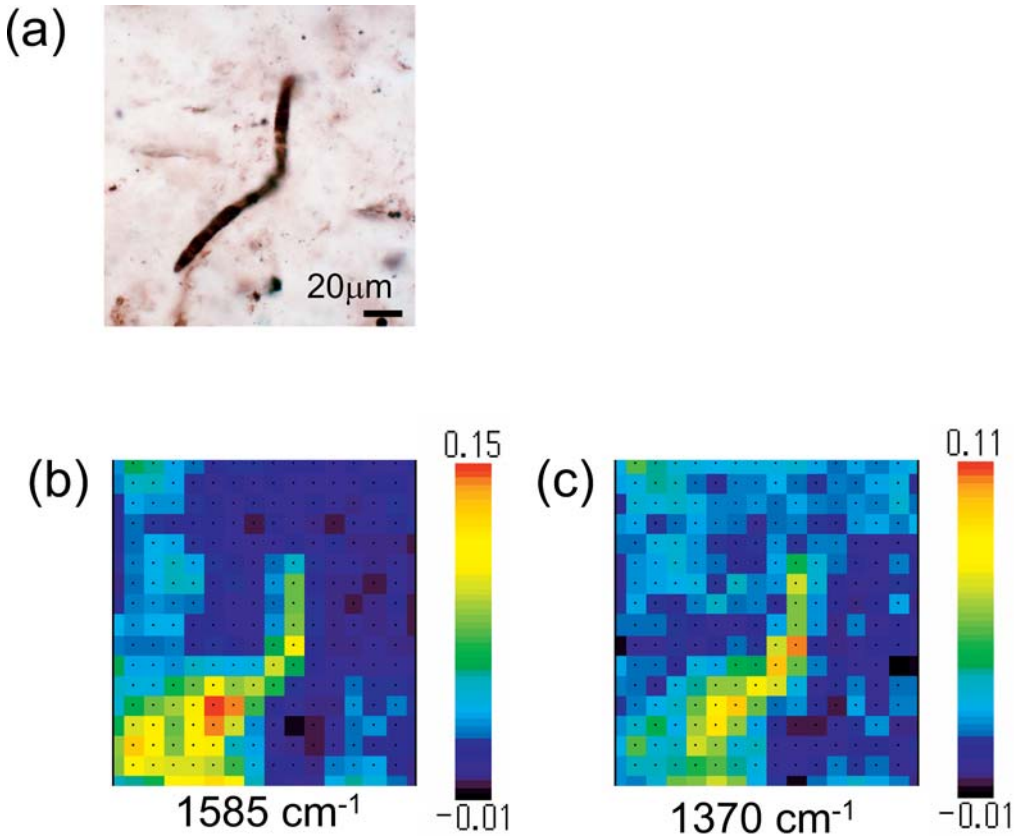

FIG. 10. IR mapping results by the IR difference spectra (Fig. 5) of the filamentous microfossil embedded in the doubly-polished petrographic thin section. (**a**) Optical photomicrograph of the measured area (170×180 μm^2). Scale bar represents 20 μm. The spatial distribution maps for the peak heights at (**b**) 1585 cm^{-1} (C–C) and (**c**) 1370 cm^{-1} (C–H). The color scale represents the higher peak height (red) and the lower one (blue) in absorbance units (AU). Analytical errors in absorbance are 0.01 AU.

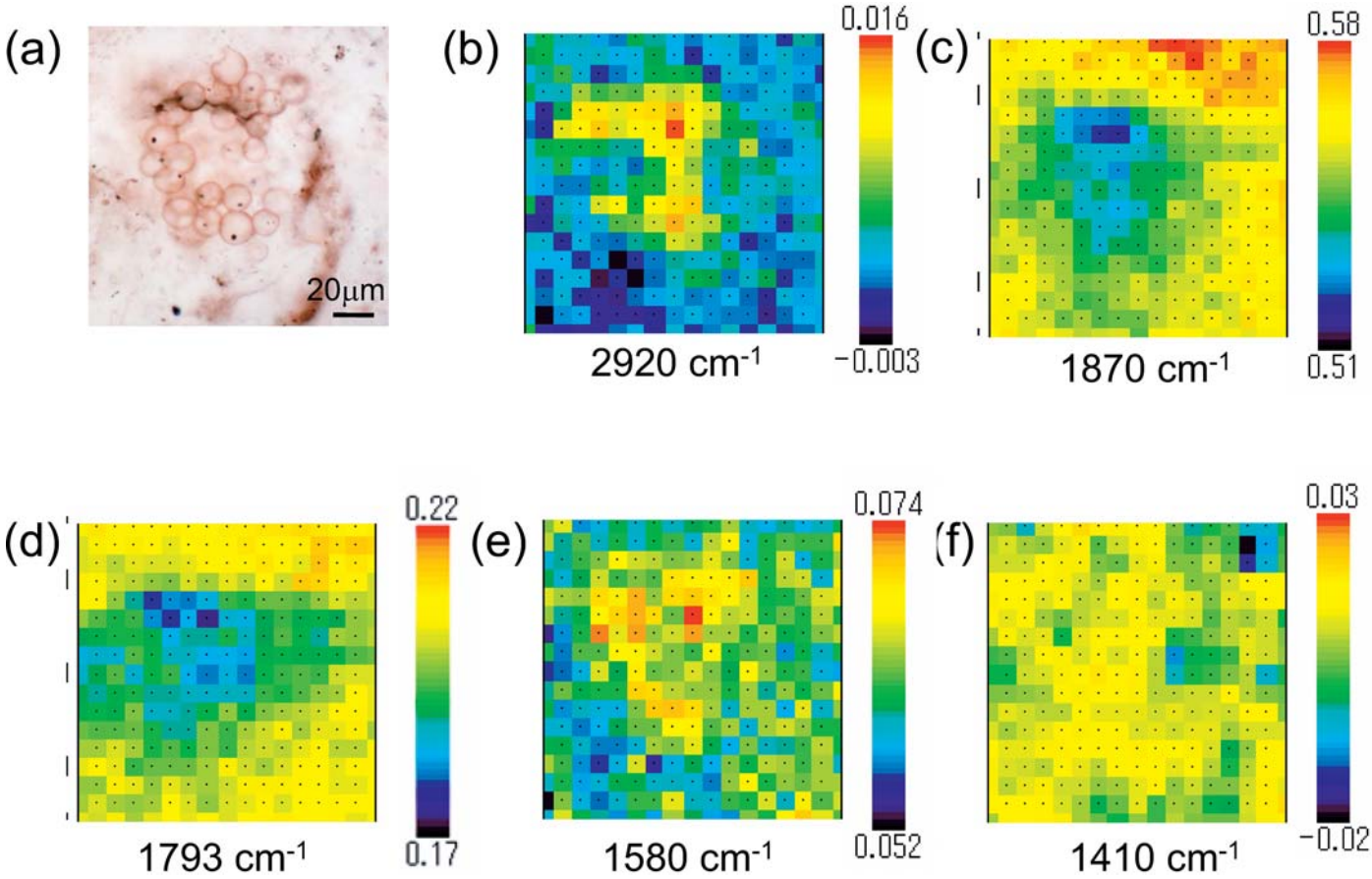

FIG. 11. IR mapping results by the raw IR transmission spectra of the coccoidal microfossils embedded in the doubly-polished petrographic thin section. (**a**) Optical photomicrograph of the measured area (170 × 180 μm^2). Scale bar represents 20 μm. The spatial distribution maps for the peak heights at (**b**) 2920 cm^{-1} (C–H), (**c**) 1870 cm^{-1} (Si–O), (**d**) 1793 cm^{-1} (Si–O), (**e**) 1580 cm^{-1} (C–C), and (**f**) 1410 cm^{-1} (C–H). The color scale represents the higher peak height (red) and the lower one (blue) in absorbance units (AU). Analytical errors in absorbance are 0.01 AU.

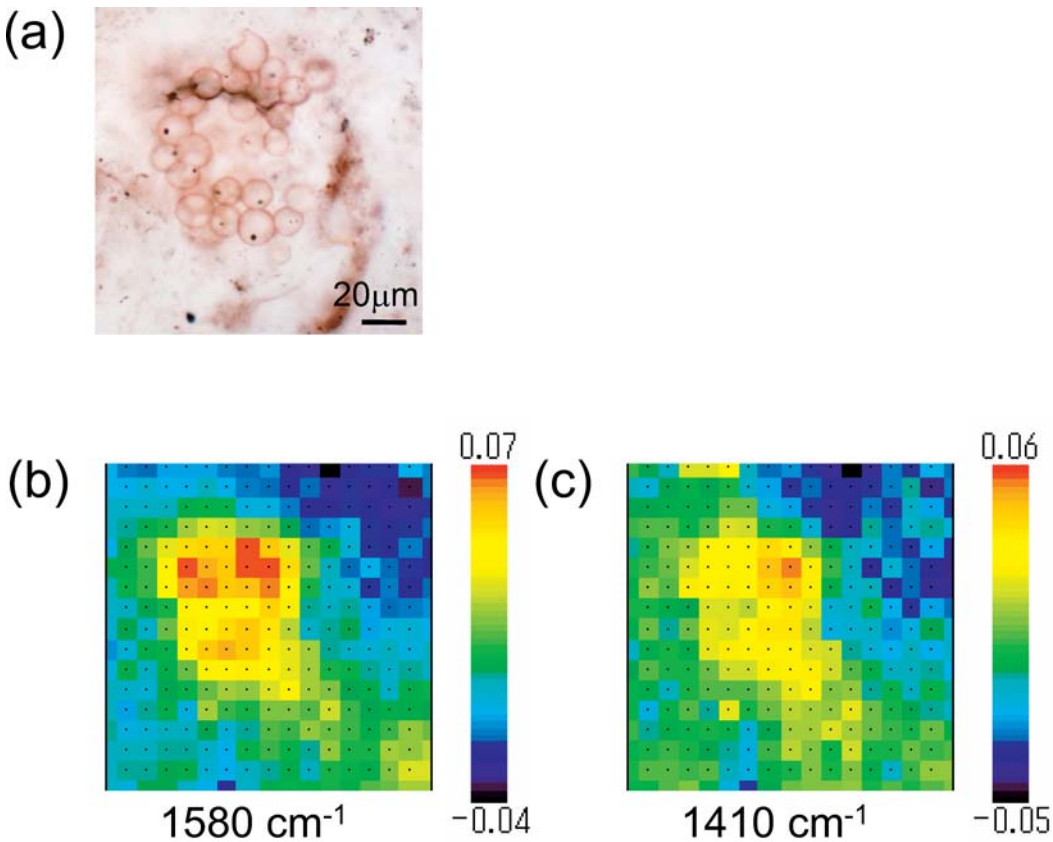

FIG. 12. IR mapping results by the IR difference spectra of the coccoidal microfossils embedded in the doubly-polished petrographic thin section. (**a**) Optical photomicrograph of the measured area (170 × 180 μm^2). Scale bar represents 20 μm. The spatial distribution maps for the peak heights at (**b**) 1580 cm^{-1} (C–C) and (**c**) 1410 cm^{-1} (C–H). The color scale represents the higher peak height (red) and the lower one (blue) in absorbance units (AU). Analytical errors in absorbance are 0.01 AU.

is called the disordered peak (D peak).[8,13] These peaks are characteristic of the C–C bond of disordered carbonaceous material. The peak around 461 cm^{-1} was due to the Si–O stretching vibration characteristic of quartz,[32] the mineral enclosing the microfossils.

Infrared Microspectroscopy. Infrared transmission spectra showed mainly the absorption by quartz (Fig. 3). Seven absorption bands at 1995, 1870, 1793, 1684, 1610, 1525, and 1492 cm^{-1} were due to overtones and combinations of Si–O vibrations and are characteristic of quartz.[33] The peak around 2350 cm^{-1} is absorption by CO_2 in air. The ranges 1290–1000 cm^{-1} (Si–O stretch) and 820–760 cm^{-1} (O–Si–O bend) are saturated due to thick samples (the 40 μm thickness of the doubly-polished rock chip). Figure 3 also shows absorption bands around 3400, 2960, 2920, and 2850 cm^{-1}. The band around 3400 cm^{-1} was due to O–H stretching vibrations. The broad 3400 cm^{-1} band is generally considered to be due to liquid-like molecular water (H_2O).[33–35] The band at 2960 cm^{-1} was due to C–H stretching vibrations of aliphatic CH_3,[36] while the 2920 and 2850 cm^{-1} bands were due to C–H stretching vibrations of aliphatic CH_2.[36]

In order to check the possibility of any of the carbon-based dissolvable adhesive (ARON ALPHA) remaining, IR transmission-reflection spectra for this adhesive on an Al plate were measured. These results showed C–H absorption bands at 2988, 2944, 2908, and 2876 cm^{-1} (Fig. 4). Since the wavenumber resolution of the IR spectrometer is 4 cm^{-1}, these bands were considered to be different from the observed C–H bands at 2960, 2920, and 2850 cm^{-1} for the filamentous microfossil (Fig. 3). The other absorption bands typical of the adhesive at 1757 cm^{-1} (Fig. 4) were not observed in the filamentous microfossil spectra. Therefore, the adhesive used to attach the rock chip to the glass was considered to be almost completely removed.

No organic signatures were recognizable in the raw IR transmission spectra in the range from 2300 to 1300 cm^{-1} (Figs. 3 and 5b). However, the IR transmission spectra for the filamentous microfossil minus that for the quartz matrix (free of amber to dark-brown materials) revealed the presence of bands around 1585 cm^{-1}, 1370 cm^{-1}, and possibly at 1450 cm^{-1} (Fig. 5c). These spectra are called here the IR difference spectra.

In order to check for artifacts due to the spectral subtraction, IR line analysis of the quartz matrix without amber to dark-brown objects was conducted against air background (Fig. 6b). The IR difference spectra from the first area (to the left in Fig. 6a) did not show absorption bands in the 2300–1300 cm^{-1} range, with some sharp noise at −0.04 to 0.19 in absorbance (Fig. 6b). The quartz matrix is fairly homogeneous in this IR difference spectral region. Therefore, the 1585, 1450, and 1370 cm^{-1} bands recognized in the IR difference spectra (Fig. 5c) are not due to artifacts of spectral subtraction.

In order to improve spectral resolution, IR transmission spectra of the filamentous microfossil were measured by accumulating 1000 scans, and a spectrum of the quartz matrix was subtracted from these in order to obtain IR difference spectra with high S/N ratios (called here high S/N IR spectra) (Fig. 7). These show fine features around the 2900 and 1400 cm^{-1} bands. A weak shoulder at 2875 cm^{-1} due to CH_3 stretch can be recognized along with 2960 (CH_3), 2920 (CH_2), and 2850 cm^{-1} (CH_2) bands. The bands around 1585, 1450, and 1370 cm^{-1} are now clearly recognizable (Fig. 7a). The negative band around 3400 cm^{-1} in Fig. 7a is considered to be due to the smaller liquid-like water content rather than the quartz matrix. On the other hand, the positive band around 3400 cm^{-1} in Fig. 7c is due to the larger liquid-like water contents. Fine wave-like features in Fig. 7a and Fig. 7c are due to interference fringes of the parallel thin section.

High S/N IR spectra of the coccoidal microfossils showed all the bands at 2960 cm^{-1} (CH_3), 2920 cm^{-1} (CH_2), 2850 cm^{-1} (CH_2), 1580 cm^{-1} (assignment will be discussed later), and 1410 cm^{-1} (CH_2 and CH_3 bend) (Figs. 5c and 5d).

Infrared transmission-reflection spectra of residues on the Pt plate after the HF/HCl treatment (Fig. 8) showed several bands around 3320, 3200, 3080, 2955, 2920, 2850, 1650, 1585, and 1420 cm^{-1}. The spectra do not have absorption bands around 1280–1010 cm^{-1} and 820–760 cm^{-1} due to Si–O (Fig. 3), indicating that quartz in the thin section was almost completely removed by the HF treatment. However, the band around 1420 cm^{-1} in the residues after HF/HCl treatment could be due to remaining carbonate.[37] The broad band around 3320 cm^{-1} with shoulders around 3200 and 3080 cm^{-1} seems to be composed of several components. The 3320, 3200, and 3080 cm^{-1} bands were possibly due to N–H, alcoholic O–H, and aromatic C–H bonds in the organic residue, respectively. The shoulder around 2960 cm^{-1} was due to C–H stretching vibration of aliphatic CH_3.[36] The bands around 2920 and 2850 cm^{-1} were due to aliphatic CH_2.[36] The 1650 cm^{-1} band might be due to the H–O–H bending vibration of adsorbed water. The attributions of bands around 1585 and 1420 cm^{-1} will be discussed later. Although most of the organic absorption bands observed in the IR spectra on the doubly-polished rock thin section were obtained from the residue, some differences were also observed.

Infrared Mapping Analysis. All the above IR spectra of the microfossils indicated the presence of organic components at 2960, 2920, and 2850 cm^{-1} (aliphatic C–H) and around 1585 and 1370 cm^{-1}. In order to clarify the distribution of these components, IR mapping analysis against air background was conducted on the filamentous and coccoidal microfossils. Although high S/N IR spectral mapping is desirable, 1000 scans for many areas needed several tens of hours of measurement, which is impossible with the 8-hour time limit imposed by liquid nitrogen for cooling the MCT detector. Therefore, 100 scans were accumulated for a 20 μm × 20 μm aperture area shifted every 10 μm over an area of about 170 μm × 180 μm. This resulted in about 280 IR spectra (about 7 hours).

The spatial distribution of peak intensity (peak height) at around 2920 cm^{-1} in raw IR transmission spectra for the filamentous microfossil is presented in Fig. 9b. The distribution of the C–H peak (2920 cm^{-1}) matches well the form of the filamentous microfossil (Fig. 9a). The distributions of the intensities of two bands at 1870 and 1793 cm^{-1} due to Si–O (Fig. 5b) showed lower parts corresponding to the positions of the filamentous microfossil (Figs. 9c and 9d). The 1585 cm^{-1} band intensities were also high for these positions (Fig. 9e). However, the shoulder band at 1370 cm^{-1} beside the large saturated Si–O band around 1000 cm^{-1} did not show a clear distribution (Fig. 9f).

In order to better resolve these shoulder bands, IR difference spectra were calculated by subtracting a quartz matrix spectrum (the 1585 and 1370 cm^{-1} bands could be observed clearly after spectral subtraction of the quartz matrix) (Fig. 7a). The peak heights at 1585 and 1370 cm^{-1} in these IR difference spectra

showed clearer distributions matching the filamentous microfossil (Figs. 10b and 10c).

Infrared mapping analysis of the coccoidal microfossils was also conducted in the same way as for the filamentous microfossil. The distributions of 2920, 1870, 1793, 1580, and 1410 cm^{-1} intensities obtained from raw IR transmission spectra of the coccoidal microfossils are shown in Figs. 11b–11f. The Si–O bands at 1870 and 1793 cm^{-1} showed lower intensities in the coccoidal microfossils than in the quartz matrix (Figs. 11c and 11d). The peak heights of the 2920 and 1580 cm^{-1} bands showed similar distributions to those of the coccoidal microfossils (Figs. 11b and 11e). However, the 1410 cm^{-1} band intensity was almost homogeneous in the measured area based on these raw IR transmission spectra. By taking IR difference spectra from a quartz matrix (Fig. 7c), the IR mapping results showed better distribution patterns for the 1580 and 1410 cm^{-1} bands (Figs. 12b and 12c) corresponding to the coccoidal microfossils (Fig. 12a).

DISCUSSION

Raman microspectroscopy of the microfossils in the doubly-polished petrographic thin section showed the presence of both graphite (G) and disordered (D) peaks (Fig. 2), suggesting that they consist of disordered carbonaceous material. The G and D band widths of carbonaceous material varied according to the degree of its maturity.[8,38] The relatively wide bandwidths of these bands in Fig. 2 indicate that the microfossils from the Bitter Springs Formation are immature carbonaceous material showing a relatively low degree of graphitization. This disordered carbonaceous structure of the microfossils might be due to the presence of polar groups among their aromatic sheet structures.

Infrared microspectroscopy indicated that the distribution of C–H bonds (2920 cm^{-1}) agreed well with the form of the filamentous microfossil (Fig. 9b). IR transmission spectra for this microfossil showed less abundant 2960 cm^{-1} band due to end methyl (CH_3) groups compared with the 2920 cm^{-1} band (C–H stretching vibration of aliphatic CH_2) (Fig. 3). Therefore, the filamentous microfossil embedded in the chert of the doubly-polished petrographic thin section retains aliphatic hydrocarbon compounds composed mainly of aliphatic chain ($–CH_2–$) groups. IR microspectroscopy on the coccoidal microfossils showed similar results on these aliphatic C–H bands.

The IR difference spectra for the filamentous microfossil against the air background showed bands around 1585 and 1370 cm^{-1} with the shoulder around 1450 cm^{-1} (Fig. 5c). Those for quartz matrix did not show such bands, except for some sharp noise in this region (Fig. 6). The high S/N IR spectrum of the same filamentous microfossil showed a clear band around 1450 cm^{-1} as well as 1370 cm^{-1} and 1585 cm^{-1} bands (Fig. 7a). Therefore, the broad band around 1370 cm^{-1} in Fig. 5c can be a mixture of several components such as the 1450 and 1370 cm^{-1} bands. On the other hand, this 1450 cm^{-1} band could not be recognized in the high S/N IR spectrum for the coccoidal microfossils showing two broad bands around 1580 and 1410 cm^{-1} (Fig. 7c). The 1585–1580 cm^{-1} band can be due to the C–C bond in the aromatic ring substituted by some polar components.[36] The 1450 cm^{-1} and 1370 cm^{-1} bands can be due to C–H bending vibration of aliphatic $CH_2 + CH_3$ and CH_3 groups, respectively.[36] The presence of 2960 and 2875 cm^{-1} shoulders due to CH_3 stretching vibration in the high S/N IR spectrum of the filamentous microfossil is consistent with the presence of the 1370 cm^{-1} band due to the CH_3 group (Fig. 7a). On the other hand, the high S/N IR spectrum of the coccoidal microfossils has relatively smaller shoulders at 2960 and 2875 cm^{-1}, and the 1370 cm^{-1} band could not be recognized (Fig. 7c). Therefore, the filamentous microfossil might contain more CH_3 groups than the coccoidal microfossils. IR transmission-reflection spectra of the residue after HF/HCl treatment showed that the 2960, 2875, and 1370 cm^{-1} bands are small (Fig. 8). The microfossils as a whole have hence mainly CH_2 groups in their structures.

The presence of polar components such as C–H in the microfossils suggests that remnants of altered biomolecules can be retained in the microfossils. The above spectral signatures might provide biological molecular records of microfossils in ancient rocks.

CONCLUSION

This study successfully applied IR microspectroscopy together with Raman microspectroscopy to small prokaryotic fossils preserved in chert in order to detect their spectral signatures. IR and Raman microspectroscopic measurements of these ~850 million-year-old filamentous and coccoidal microfossils from the Bitter Springs Formation of central Australia produced the following spectral signatures:

(1) Raman microspectroscopy on the microfossils shows the presence of both graphite (G) and disordered (D) bands, indicating that they consist of disordered carbonaceous compounds.

(2) IR microspectroscopy of the microfossils shows the presence of the 2920 (CH_2) and 2850 cm^{-1} (CH_2) bands, and IR mapping indicates that the distribution of peak intensity at the 2920 cm^{-1} band agrees well with the morphology of the microfossils. The filamentous microfossil shows shoulders at 2960 and 2875 cm^{-1} due to CH_3 groups, while these bands are not clear for the coccoidal microfossils.

(3) The distributions of IR peak intensities of the 1585 and 1370 cm^{-1} bands agree roughly with the morphology of the filamentous microfossil. These bands can be due to the aromatic C–C bond substituted by polar components and the aliphatic CH_3 group, respectively.

(4) The IR bands around 1580 and 1410 cm^{-1} from the coccoidal microfossils can be attributed to aromatic C–C bonds substituted by polar components and the aliphatic CH_2 group, respectively.

Based on the above IR and Raman microspectroscopic results, the filamentous and coccoidal microfossils from the ~850 Ma Bitter Springs Formation retain functional groups such as aromatic C–C substituted by polar components and aliphatic C–H. Therefore, IR microspectroscopy is able to detect *in situ* some organic polar signatures in prokaryotic fossils embedded in doubly-polished petrographic thin sections. This method should serve as a powerful technique to determine the likely biological origin of putative microfossils.

ACKNOWLEDGMENTS

We would like to thank all the members of Maruyama, Hirose, and Nakashima laboratories for their helpful advice and suggestions on this study. We also thank Jasco Co, Ltd. for their technical support of the Raman and IR microspectroscopic analyses. M.I. is grateful to Yoshida Scholarship Foundation for their financial support. The major part of this study was conducted at the Department of Earth and Space Science, Osaka University. This research was partly supported by the 21st Century COE program "How to build habitable planets", Tokyo Institute of Technology, sponsored by the Ministry of Education, Culture, Sports, Technology and Science, Japan.

1. J. W. Schopf and M. R. Walter, "Archean Microfossils: New Evidence of Ancient Microbes", in *The Earth's Earliest Biosphere: Its Origin and Evolution* (Princeton University Press, Princeton, New Jersey, 1983), p. 214.
2. R. Buick, Palaios **5,** 441 (1990).
3. J. W. Schopf, A. B. Kudryavtsev, D. G. Agresti, A. D. Czaja, and T. J. Wdowiak, Astrobiology **5,** 333 (2005).
4. S. M. Awramik, J. W. Schopf, and M. R. Walter, Precambrian Res. **20,** 357 (1983).
5. J. W. Schopf, Science (Washington, D.C.) **260,** 640 (1993).
6. A. B. Kudryavtsev, J. W. Schopf, D. G. Agresti, and T. J. Wdowiak, PNAS **98,** 823 (2001).
7. Y. Ueno, Y. Isozaki, H. Yurimoto, and S. Maruyama, Int. Geol. Rev. **43,** 196 (2001).
8. J. W. Schopf, A. B. Kudryavtsev, D. G. Agresti, T. J. Wdowiak, and A. D. Czaja, Nature (London) **416,** 73 (2002).
9. M. D. Brasier, O. R. Green, A. P. Jephcoat, A. K. Kleppe, M. J. Van Kranendonk, J. F. Lindsay, A. Steele, and N. V. Grassineau, Nature (London) **416,** 76 (2002).
10. J. D. Pasteris and B. Wopenka, Nature (London) **420,** 476 (2002).
11. M. D. Brasier, O. Green, J. F. Lindsay, and A. Steele, Origins Life Evol. Biosphere **34,** 257 (2004).
12. K. Grey, "A modified palynological preparation technique for the extraction of large Neoproterozoic acanthomorph acritarchs and other acid-insoluble microfossils", Western Australia Geological Survey, Record 1999/10, p. 23.
13. J. D. Pasteris and B. Wopenka, Astrobiology **3,** 727 (2003).
14. S. Nakashima, J. R. Disnar, A. Perruchot, and J. Trichet, Geochim. Cosmochim. Acta **48,** 2321 (1984).
15. S. Nakashima, Sci. Total Environ. **117/118,** 425 (1992).
16. S. Nakashima, Org. Geochem. **19,** 421 (1992).
17. F. J. Stevenson, *Spectroscopic Approarches. Humus Chemistry: Genesis, Composition, Reactions* (John Wiley and Sons, New York, 1994), 2nd ed., p. 303.
18. G. Zubay, *Origins of Life on the Earth and in the Cosmos* (Academic Press, San Diego, 2000), 2nd ed., p. 564.
19. K. Arouri, P. F. Greenwood, and M. R. Walter, Org. Geochem. **30,** 1323 (1999).
20. K. Arouri, P. F. Greenwood, and M. R. Walter, Org. Geochem. **31,** 75 (2000).
21. C. P. Marshall, E. J. Javaux, A. H. Knoll, and M. R. Walter, Precambrian Res. **138,** 208 (2005).
22. K. Nakamura, M. E. Zolensky, S. Tomita, S. Nakashima, and K. Tomeoka, Int. J. Astrobiol. **1(3),** 179 (2002).
23. K. Artyushokova, B. Wall, J. L. Koenig, and J. E. Fulghum, Appl. Spectrosc. **54,** 1549 (2000).
24. A. J. Sommer, L. G. Tisinger, C. Marcott, and G. M. Story, Appl. Spectrosc. **55,** 252 (2001).
25. I. Keen, L. Rintoul, and P. M. Fredericks, Appl. Spectrosc. **55,** 984 (2001).
26. A. Gupper, P. Wilhelm, M. Schmied, S. G. Kazarian, K. L. A. Chan, and J. Reubner, Appl. Spectrosc. **56,** 1515 (2002).
27. C. H. House, J. W. Schopf, K. D. McKeegan, S. D. Coath, T. M. Harrison, and K. O. Stetter, Geology **28,** 707 (2000).
28. M. R. Walter, J. J. Veevers, C. R. Calver, P. Gorjan, and A. C. Hill, Precambrian Res. **100,** 371 (2000).
29. E. S. Barghoorn and J. W. Schopf, Science (Washington, D.C.) **150,** 337 (1965).
30. J. W. Schopf, J. Paleontol. **42,** 651 (1968).
31. J. W. Schopf and J. M. Blacic, J. Paleontol. **45,** 925 (1971).
32. P. F. McMillan, J. Dubessy, and R. Hemley, "Applications in Earth, Planetary and Environmental Sciences", in *Raman Microscopy Developments and Applications*, G. Turrell and J. Corset, Eds. (Academic Press, London, 1996), Chap. 7, p. 289.
33. Y. Ito and S. Nakashima, Chem. Geol. **189,** 1 (2002).
34. R. S. Aines and G. R. Rossman, J. Geophys. Res. **89,** 4059 (1984).
35. A. K. Kronenberg, *Hydrogen Speciation and Chemical Weakening of Quartz, in Silica: Reviews in Mineralogy*, P. J. Heaney, C. T. Prewitt, and G. V. Gibbs, Eds. (Mineralogical Society of America, Washington, D.C., 1994), vol. 29, p. 123.
36. L. J. Bellamy, *The Infra-red Spectra of Complex Molecules* (John Wiley and Sons, New York, 1954), p. 13.
37. H. Komada, *Infrared Spectra of Minerals: Reference Guide to Identification and Characterization of Minerals for the Study of Soils* (Research Branch Agriculture, Canada, 1985), p. 28.
38. B. Wopenka and J. D. Pasteris, Am. Mineral. **78,** 533 (1993).